

# RSC Advances



This is an *Accepted Manuscript*, which has been through the Royal Society of Chemistry peer review process and has been accepted for publication.

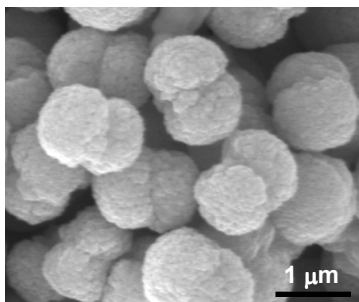
*Accepted Manuscripts* are published online shortly after acceptance, before technical editing, formatting and proof reading. Using this free service, authors can make their results available to the community, in citable form, before we publish the edited article. This *Accepted Manuscript* will be replaced by the edited, formatted and paginated article as soon as this is available.

You can find more information about *Accepted Manuscripts* in the [Information for Authors](#).

Please note that technical editing may introduce minor changes to the text and/or graphics, which may alter content. The journal's standard [Terms & Conditions](#) and the [Ethical guidelines](#) still apply. In no event shall the Royal Society of Chemistry be held responsible for any errors or omissions in this *Accepted Manuscript* or any consequences arising from the use of any information it contains.

**Graphical Abstract:**

**Complex Twin-Microspheres:** Metal oxide hierarchical twin-spheres were synthesized by a general strategy involving the solution synthesis of metal carbonate twin-spheres and subsequent thermal annealing. Their structural features cause an excellent electrochemical performance as advanced electrode materials for lithium-ion batteries.

**TOC figure**

## General Formation of Mn-based Transition Metal Oxide Twin-Microspheres with Enhanced Lithium Storage Properties

Yurong Liu,<sup>a,b</sup> Bochen Zhang,<sup>a</sup> Jinkui Feng,<sup>a</sup> and Shenglin Xiong<sup>a,\*</sup>

<sup>a</sup>Key Laboratory for Colloid and Interface Chemistry & Key Laboratory of Special Aggregated Materials, Ministry of Education, and School of Chemistry and Chemical Engineering, Shandong University, Jinan 250100, P. R. China

<sup>b</sup>School of Resources and Environmental Engineering, Shandong University of Technology, Zibo, Shandong, 255049, PR China

Email: [chexsl@sdu.edu.cn](mailto:chexsl@sdu.edu.cn)

**Abstract:** In this investigation, we designed a general method to manipulate the controlled preparation of Mn-based transition metal oxide materials with structure of hierarchical twin-microspheres. Initiated by the precursor synthesis of metal carbonate twin-microspheres obtained solvothermally, the formation of hierarchical twin-microspheres of metal oxides was finalized by thermal annealing in laboratory air. The method allows one to prepare binary and ternary hierarchical twin-microspheres constructed by primary ultrathin nanoparticles. By applying the respective metal salts in synthesis, six oxide species, including  $\text{Mn}_3\text{O}_4$ ,  $\text{CoMn}_2\text{O}_4$ ,  $\text{ZnMn}_2\text{O}_4$ ,  $\text{Ni}_x\text{Mn}_{3-x}\text{O}_4$ ,  $\text{Cu}_x\text{Mn}_{3-x}\text{O}_4$ , and  $\text{Fe}_x\text{Mn}_{3-x}\text{O}_4$ , have been reported herein in order to draw common features via oriented-attachment. Concerning the workability,  $\text{CoMn}_2\text{O}_4$  twin-microspheres are evaluated as electrode materials for lithium-ion batteries. As expected, the  $\text{CoMn}_2\text{O}_4$  twin-microspheres exhibit excellent rate performance and impressive cycling stability due to their unique assembled architecture and probably synergetic effects of different metal ions.

**Keywords:** mixed metal oxides, twin-spheres, nanostructures, general formation, Lithium-ion batteries, anodes

## 1. Introduction

Recently, transition metals oxides (TMOs), especially the group of mixed valence oxides, attracted research focus due to the high theoretical capacity. Their applications in energy storage devices range from oxygen reduction reaction (ORR), electrochemical capacitors (ECs) to LIBs.<sup>1-11</sup> Amongst the 3d transition metal oxide anodes, Mn-based TMOs have been given notable attention owing to their advantages of low cost, abundance and environmental friendliness, high capacity and low operating voltage and so on. Myriad micro/nanostructures of Mn-based binary and ternary oxides, such as MnO,<sup>12-15</sup> Mn<sub>3</sub>O<sub>4</sub>,<sup>16-19</sup> CoMn<sub>2</sub>O<sub>4</sub><sup>8-10</sup> and ZnMn<sub>2</sub>O<sub>4</sub>,<sup>8,20-23</sup> have been successfully synthesized and excellent lithium storage properties have been obtained. In fact, the real performance of electrodes always encountered some issues, such as poor cycling profile, low rate capability, and high operating voltage.<sup>24</sup> As established by related research, porous architectures assembled by numerous subclasses of nano-building blocks opened up accessible route to enhance behaviors of reverse capacity and rate capability.<sup>8-11,20,25</sup> In this scenario, higher surface area offered adequate contact sites between electrode and electrolyte. The porous configuration served as free transportation channels for Li ions to move into bulk of electrode, shortening the whole diffusion duration. Furthermore, assembled structure could well buffer the volume variation to maintain the good mechanical strength during the repeated lithium ions insertion/extraction processes.

Considering the gigantic potential of porous architectures in LIBs, to rationally engineer the formation of porous micro/nanocomposite materials with novel structures became a challenging task in the nanochemistry community.<sup>26-30</sup> As a kind of special micro/nanostructure, twin-spheres with various architectures have been fabricated through different synthesis routes.<sup>20,25,31,32</sup> For example, Li and coworkers fabricated  $\text{Co}_3\text{O}_4$  twin-microspheres with an urchin-like structure based on a mechanism of multistep-splitting growth from 1D nanorods and observed an enhanced specific capacitances for supercapacitors.<sup>32</sup> 3D  $\text{ZnCo}_2\text{O}_4$  hierarchical twin microspheres were produced via a typical combined process of multistep splitting and in-situ dissolution-recrystallization, offering a reversible capacity of  $550 \text{ mAh g}^{-1}$  at a rate of  $5 \text{ A g}^{-1}$  after 2000 cycles when evaluated as anode materials for lithium-ion batteries (LIBs).<sup>25</sup> Notwithstanding these advancements, the synthesis of twin-spheres with hierarchical micro/nanostructures is still in a rudimentary state of development by comparison with what has been achieved for their spherical counterparts. Moreover, most synthetic strategies showed accessibility only to the formation of one certain material in their respective processes. Accordingly, it would be highly desirable to develop a feasible, but general strategy to effectively synthesize porous twin-spheres with a relatively general formation mechanism for different functional materials.

In view of considerations and inspiration mentioned above, herein, a

general route had been developed to fabricate hierarchical porous Mn-based oxide ( $A_xMn_{3-x}O_4$ ,  $0 \leq x < 3$ ; A = Co, Zn, Ni, Cu, Fe) twin-microspheres via a multiple strategy consisting of modified polyol avenue and subsequent thermal process. To be exact, taking  $CoMn_2O_4$  as an example, monodisperse  $Co_{0.33}Mn_{0.67}CO_3$  twin microspheres have been firstly synthesized via an oriented-attachment accompanied by Ostwald ripening.  $CoMn_2O_4$  twin microspheres were then fabricated by annealing the above precursor at  $500\text{ }^\circ\text{C}$  for 4 h in laboratory air. To the best of our knowledge, this is the first report on the preparation of  $CoMn_2O_4$  twin microspheres via a simple solution-based route. When evaluated as anode materials for LIBs, these new  $CoMn_2O_4$  twin-microspheres exhibit high specific capacity with excellent rate capability and enhanced cycling stability, making them potential electrode for LIBs. As the current synthetic strategy was extended to prepare  $Mn_3O_4$ ,  $ZnMn_2O_4$ ,  $Ni_xMn_{3-x}O_4$ ,  $Cu_xMn_{3-x}O_4$ , and  $Fe_xMn_{3-x}O_4$ , similar twin microspheres have been successfully realized.

## 2. Experimental Section

**Chemicals:** triethylene glycol (TEG, absolute for analysis) was purchased from Wuxi Zhanwang Chemical Reagent Co. Ltd in China. All the following reagents were supplied by Shanghai Sinopharm Chemical Reagent Co. Ltd.: manganese acetate tetrahydrate ( $Mn(Ac)_2 \cdot 4H_2O$ , 99%, AR), cobalt acetate tetrahydrate ( $Co(Ac)_2 \cdot 4H_2O$ , 99%, AR), zinc acetate dihydrate ( $Zn(Ac)_2 \cdot 2H_2O$ , 99%, AR), cobalt acetate tetrahydrate ( $Ni(Ac)_2 \cdot 4H_2O$ , 99%, AR), copper

acetate monohydrate ( $\text{Cu}(\text{Ac})_2 \cdot \text{H}_2\text{O}$ , 99%, AR), iron oxalate dehydrate ( $\text{FeC}_2\text{O}_4 \cdot 2\text{H}_2\text{O}$ , 99%, AR) and  $\text{NH}_4\text{HCO}_3$  (99%, AR). All chemicals are directly used without any treatment.

**Synthesis of  $\text{CoMn}_2\text{O}_4$  twin-microspheres:** In a typical synthesis, 0.5 mmol of  $\text{Co}(\text{Ac})_2 \cdot 4\text{H}_2\text{O}$  and 1 mmol of  $\text{Mn}(\text{Ac})_2 \cdot 4\text{H}_2\text{O}$  are firstly dissolved into 40 mL of TEG to form a transparent solution under magnetic stirring for 30 min. Then, 30 mmol of  $\text{NH}_4\text{HCO}_3$  powder was added to the above mixture. The resultant mixture was continually stirred until getting a homogeneous solution and then transferred into a Teflon lined stainless-steel autoclave (capacity of 50 mL). The autoclave was sealed and maintained at 200 °C for 20 h in an electronic oven. After reaction, the system cooled down to ambient temperature naturally. The obtained product (analyzed as  $\text{Co}_{0.33}\text{Mn}_{0.67}\text{CO}_3$  twin-microspheres in the main text) was harvested by centrifugation and washed with water and ethanol for several times. Followed by heat post-treatment at 500 °C under laboratory air for 4 h with a ramp rate of  $1\text{ }^\circ\text{C} \cdot \text{min}^{-1}$ , targeted  $\text{CoMn}_2\text{O}_4$  twin-microspheres could be obtained.

Other Mn-based metal oxides were prepared with the similar procedures as that used for  $\text{CoMn}_2\text{O}_4$  twin-microspheres except for using different metal acetate/oxalate precursors, which would be specified in the following text.

**Materials Characterization:** The crystallographic phase of as-synthesized samples was characterized by powder X-ray diffraction (XRD, Philips X'Pert Pro Super diffractometer, Cu K $\alpha$  radiation  $\lambda = 1.54178\text{ \AA}$ ). Morphological and

structural investigations were carried out with Field-emission scanning electron microscopy (FESEM, JSM-6300F, JEOL). Structural and compositional information was provided by transmission electron microscopy (TEM), high-resolution TEM (HRTEM), and affiliated energy-dispersive X-ray spectroscopy (EDX) operated with an accelerating voltage of 200 kV (JEM-2010 and JEM-2100F, JEOL). Surface analysis of the samples was detected by X-ray photoelectron spectroscopy (XPS, AXIS-HSi, Kratos Analytical) and the binding energies were calibrated using C1s peak (284.6 eV) as a reference.

**Electrochemical Measurements:** The active material ( $\text{CoMn}_2\text{O}_4$  twin-spheres), conductive material (acetylene black), and polymer binder (Carboxy Methylated Cellulose, CMC,) were milled for 3 h at a weight ratio of 70:20:10, and then coated on the surface of a copper foil. The working electrode had the diameter of 12 mm, with coating thickness of 200  $\mu\text{m}$  and the density of the active material is about 1.0  $\text{mg cm}^{-2}$ . The electrochemical measurements were carried out using 2032 coin cells with lithium foil as both the counter and reference electrodes. 1 M  $\text{LiPF}_6$  in a mixture of ethylene carbonate (EC), dimethylcarbonate (DMC) and diethyl carbonate (DEC) (1:1:1, v/v/v) was used as the electrolyte. The cell was assembled in an Argon-filled glovebox with both the moisture and the oxygen content below 1 ppm. The galvanostatic charge/discharge data were collected by CT2001A LAND Cell test system at different current densities. The cyclic voltammetry (CV) was

tested within the voltage range from 0.01 to 3.0 V by an electrochemical workstation (CHI760D).

### 3. Results and Discussion

Our strategy for the formation of mixed-metal-oxide complex twined structures is depicted in Figure 1, taking  $\text{CoMn}_2\text{O}_4$  as an example. According to the synthetic process outlined, monodisperse  $\text{Co}_{0.33}\text{Mn}_{0.67}\text{CO}_3$  twin microspheres, namely the precursor, formed through the following three steps: (i) the formation of randomly dispersive spheres coexisting with discrete small nanoparticles, (ii) the alignment between two spheres with the assistance of TEG ligands (light yellow thin lines between two spheres) and (iii) formation of the twin-spheres based on an oriented-attachment accompanied by Ostwald ripening with expense of small nanoparticles, (also see Figure S1-S2, Supporting Information). The resembled crystallographic nature and crystallization habits of  $\text{CoCO}_3$  and  $\text{MnCO}_3$  made them coprecipitate. XRD pattern in Figure S1 confirmed the hexagonal-phase  $\text{Co}_{0.33}\text{Mn}_{0.67}\text{CO}_3$ , similar to  $\text{CoCO}_3$  (78-0278) and  $\text{MnCO}_3$  (86-0172). Figure 3(a,b) are typical field-emission scanning electron microscopy (FESEM) images of as-formed  $\text{Co}_{0.33}\text{Mn}_{0.67}\text{CO}_3$  twin microspheres with average diameter of  $\sim 2.0 \mu\text{m}$ , clearly describing the panoramic morphological profile and demonstrating the high yield close to 100%. More materials detection by TEM can be found in the Supporting Information (Figure S2).

After calcinations treatment in laboratory air, the XRD pattern (Figure 2a) of

the final product can be readily assigned to body-centered-tetragonal  $\text{CoMn}_2\text{O}_4$  (JCPDS card no.77-0471,  $a = b = 5.784 \text{ \AA}$ ,  $c = 9.091 \text{ \AA}$ ,  $\alpha = \beta = \gamma = 90^\circ$ ; space group:  $I4_1/amd$ ) with a distorted spinel structure due to the well-known Jahn-Teller effect of manganese (III). No residues or contaminants have been detected, showing the high purity of the sample. The schematic crystal structure of spinel  $\text{CoMn}_2\text{O}_4$  is inserted in Figure 2a. In the spinel structure, the bivalent Co-ions and trivalent Mn-ions occupy the tetrahedral and octahedral void sites, which are isostructural to  $\text{Co}_3\text{O}_4$ . The more detailed elemental composition and the oxidation state of the as-obtained  $\text{CoMn}_2\text{O}_4$  are further examined by X-ray photoelectron (XPS) measurements and the corresponding results are shown in Figure 2b-d. All of the binding energies (BEs) in this XPS analysis were corrected for specimen charging by referencing them to the C 1s peak (set at 284.6 eV). By using a Gaussian fitting method, the Co 2p emission spectrum (Figure 2b) was best fitted with two spin-orbit doublets characteristic of  $\text{Co}^{2+}$  and  $\text{Co}^{3+}$ , and two shakeup satellites (shown as "Sat.").<sup>33</sup> The Mn 2p was also fitted with two spin-orbit doublets, characteristic of  $\text{Mn}^{2+}$  and  $\text{Mn}^{3+}$ , and two little shakeup satellites.<sup>34</sup> The high-resolution spectrum for the O 1s region (Figure 2d) shows three oxygen contributions. Specifically, the peak at 529.8 eV is typical of metal-oxygen bonds.<sup>35,36</sup> The peak sitting at 531.3 eV is usually associated with a higher number of defect sites with low oxygen coordination often observed in materials with small particles.<sup>37,38</sup> The peaks at  $\sim 532.4 \text{ eV}$  can be

attributed to multiplicity of physi- and chemi-sorbed water at or near the surface.<sup>35,36</sup> These data supplied the surface chemical information of CoMn<sub>2</sub>O<sub>4</sub> twin-spheres, composed of different-valence ions involving Co<sup>2+</sup>, Co<sup>3+</sup>, Mn<sup>2+</sup>, and Mn<sup>3+</sup>. Furthermore, the atomic ratio of Co to Mn elements measured from the EDX pattern (Figure S3) of the final product is very close to 1:2 from different regions detected. According to the above analysis, one can safely conclude that the cobalt manganese oxide samples prepared in this work have the chemical composition of CoMn<sub>2</sub>O<sub>4</sub> with a spinel structure.

Despite the high temperature post-treatment, CoMn<sub>2</sub>O<sub>4</sub> sample still retained the spherical morphology and size of its carbonate precursor, as revealed by the panoramic FESEM image of Figure S4 in Supporting Information. High-magnification FESEM examination (Figure 3c,d) clearly indicated the detailed structural configuration of as-obtained twin microspheres, composed of numerous uniform nanosized primary nanoparticles. A typical TEM image in Figure 3e clarified the porous features constructed by stacking nanoparticles, which is consistent with the observation of the FESEM findings. A locally magnified HRTEM image of several nanoparticles of a CoMn<sub>2</sub>O<sub>4</sub> twin microspheres recorded for Figure 3f reveals lattice fringes with interplane spacings of 0.27 nm, corresponding to the (103) planes of spinel CoMn<sub>2</sub>O<sub>4</sub>. Considering the commensurate lattice fringes, it should be noted that different single-crystalline CoMn<sub>2</sub>O<sub>4</sub> grains were also well interconnected, maintaining the same crystallographic orientation, which could enhance the required

charge transfer and thus the electron conductivity during LIB operation. In Figure 3g, elemental mapping study on a single twin-microsphere further confirms the uniform distributions of elemental Mn, Co, and O in the  $\text{CoMn}_2\text{O}_4$  hierarchical twin-microspheres.

Mixed metal oxides have been considered as a promising class of electrode materials for high-performance energy storage devices. To demonstrate the potential application of such novel complex porous structure,  $\text{CoMn}_2\text{O}_4$  twin microspheres are evaluated as electrode materials for LIBs. Figure 4a shows the first five consecutive cyclic voltammograms (CVs) at a scan rate of  $0.2 \text{ mV s}^{-1}$  in the potential range of 0.01-3.0 V. The CV curves for the first cycle are obviously different from those for the following cycles, and no significant alteration is seen from the second cycle onwards. As for the 1<sup>st</sup> cycle, the broad peak centered at  $\sim 1.25 \text{ V}$  and the sharp reduction peak at  $\sim 0.4 \text{ V}$  in the cathodic process could be attributed to the reduction of  $\text{Mn}^{3+}$  to  $\text{Mn}^{2+}$  as well as  $\text{Mn}^{2+}$  and  $\text{Co}^{2+}$  to metallic Mn and Co, respectively. Additionally, the peak at  $0.76 \text{ V}$  can be ascribed to their irreversible decomposition of solvent in the electrolyte to form the solid-electrolyte interface (SEI). In the conjugated anodic processes, two oxidation peaks at  $1.35 \text{ V}$  and  $1.99 \text{ V}$  originated from the oxidation of Mn and Co to  $\text{Mn}^{2+}$  and  $\text{Co}^{2+}$ , respectively.<sup>39</sup> From the second cycle onwards, the repeated reduction–oxidation of MnO and CoO lead to two pairs of distinct redox peaks at  $0.49/1.40 \text{ V}$  and  $1.01/2.03 \text{ V}$ , respectively. Furthermore, these CV curves mostly overlapped, demonstrating

the good cyclability and stability for the insertion and extraction of lithium ions. On the basis of analyses derived from CVs, the entire electrochemical process for  $\text{CoMn}_2\text{O}_4$  electrode can be classified as follows:

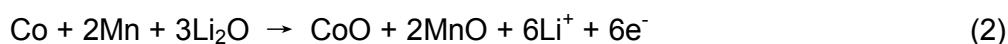
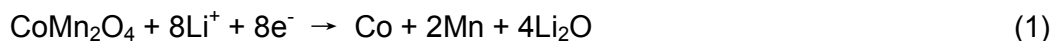


Figure 4b indicates the pertinent charge–discharge voltage profiles at a current density of  $200 \text{ mA g}^{-1}$ . The  $\text{CoMn}_2\text{O}_4$  electrode delivers high first-cycle discharge and charge capacities of  $1181$  and  $831 \text{ mAh g}^{-1}$ , respectively, contributing to a moderate irreversible loss of about 30% mainly caused by the formation of SEI during the first charge. In the following cycles, the Coulombic efficiency quickly increased to higher than 98%, showing the good cycling stability.

Figure 4c indicates the discharge/charge capacity as a function of cycle number explored at a current of  $200 \text{ mA g}^{-1}$ . Just as analyzed above, a gradual capacity loss happened due to the SEI layer formed on the electrode surface and the compact electric contact established between the current collector and electrode in the initial cycles. Afterwards, the electrode displays a stable cycling performance with high Coulombic efficiency, wherein it still remains a reversible capacity of  $890 \text{ mA h g}^{-1}$  and nearly 100% capacity retention after more than 70 cycles. Even at a high current density of  $1000 \text{ mA g}^{-1}$ , a reversible discharge capacity of  $573 \text{ mA h g}^{-1}$  is retained after continuous cycling for more than 50 cycles, corresponding to 77% of the second-cycle

discharge capacity (Figure S5, Supporting Information), much higher than the previous reports.<sup>18,19,39-41</sup> The rate capability is further evaluated at different current densities ranging from 200 to 2000 mA g<sup>-1</sup>. As seen in Figure 4d, the specific capacities are 790, 740, 664, 580, and 500 mA h g<sup>-1</sup> at the current densities of 500, 800, 1000, 1500, and 2000 mA g<sup>-1</sup>, respectively. Noticeably, when the current rate turns back to 200 mA g<sup>-1</sup>, the capacity can recover as high as 908 mA h g<sup>-1</sup> even after 120 cycles without any loss.

The lithium storage properties achieved in the present study are superior to that of other CoMn<sub>2</sub>O<sub>4</sub> structure reported.<sup>18,19,39-41</sup> For instance, the reversible capacity of the CoMn<sub>2</sub>O<sub>4</sub> hierarchical microspheres remains 894 mA h g<sup>-1</sup> at a current of 100 mA g<sup>-1</sup> after 65 cycles,<sup>18</sup> CoMn<sub>2</sub>O<sub>4</sub> hollow microcubes exhibited a capacity of about 624 mA h g<sup>-1</sup> with retention of about 75.5% at a current of 200 mA g<sup>-1</sup> after 50 cycles,<sup>33</sup> and CoMn<sub>2</sub>O<sub>4</sub> powders only indicated a capacity of 515 mA h g<sup>-1</sup> with retention of about 64% at a current of 69 mA g<sup>-1</sup> after 50 cycles. Obviously, the unique structure of present CoMn<sub>2</sub>O<sub>4</sub> complex porous structures is beneficial for enhanced lithium storage properties. Specifically, the integration of smaller primary nanoparticles and pores in the CoMn<sub>2</sub>O<sub>4</sub> twin microspheres can provide a short pathway for Li<sup>+</sup> ion diffusion, leading to high capacity and excellent rate capability. More importantly, the unique porous architecture furnished CoMn<sub>2</sub>O<sub>4</sub> twin microspheres with better structural integrity by partially alleviating the mechanical strain and the large volume change associated with the repeated Li<sup>+</sup> insertion/extraction processes during

cycling, thus lightening the pulverization problem and improving the cycling stability. It should be noted that the twin hierarchical architecture possesses lower surface energy, which can effectively inhibit self-aggregation during the charge/discharge process. Moreover, the enhanced activity is also related to the possible synergetic effects of different metal ions.

More importantly, the strategy used here shows good versatility and can be extended to the exploitation of other Mn-based metal oxides. To be specifically,  $\text{Mn}_3\text{O}_4$ ,  $\text{ZnMn}_2\text{O}_4$ ,  $\text{Ni}_x\text{Mn}_{3-x}\text{O}_4$ ,  $\text{Cu}_x\text{Mn}_{3-x}\text{O}_4$ , and  $\text{Fe}_x\text{Mn}_{3-x}\text{O}_4$  twin-microspheres are successfully synthesized by simply using their respective metal salts under same conditions. Figure 5-8 indicates the typical FESEM, TEM, and corresponding mapping images of  $\text{Mn}_3\text{O}_4$  (Figure 5a,b),  $\text{ZnMn}_2\text{O}_4$  (Figure 5c,d),  $\text{Ni}_x\text{Mn}_{3-x}\text{O}_4$  (Figure 6),  $\text{Cu}_x\text{Mn}_{3-x}\text{O}_4$  (Figure 7), and  $\text{Fe}_x\text{Mn}_{3-x}\text{O}_4$  (Figure 8) porous twin microspheres. As can be seen, similar twin-spherical structures can be prepared in large scale and high yield for these five different Mn-based metal oxides. The surfaces of the as-obtained products become much rougher than those of the corresponding precursors, suggesting the generation of porous structures. The corresponding XRD and EDX characterization can be found in the Supporting Information (Figure S6 and S7). The morphological features are quite analogous in terms of both size and shape to  $\text{CoMn}_2\text{O}_4$  twin microspheres. These interesting porous twinned structures built from nanometer-sized building blocks may offer new opportunity for applications involving areas of solar cells, electrocatalysts, supercapacitors and LIBs. Since

the present work is focused largely on the development of general routes to synthesize Mn-involved oxide twin spheres and exploit the application in LIBs with  $\text{CoMn}_2\text{O}_4$  as an example. Therefore, substantial verification of the relevant performances of other Mn-based mixed oxides will be supplied here. Although all of the twined structures in this study are exclusively Mn-based transition metal oxide, our preliminary results indicate that it would be possible to impart versatility to other transition metal oxide twin-spheres by precisely adjusting and controlling the experimental parameters, such as the composition of the solvent, the appropriate surfactant, chelating agent, the reaction temperature, and the reaction time. This versatile and controllable synthesis approach could provide a venue to fully optimize the structure and performance of complex porous twined structures.

#### 4. Conclusions

In summary, we have successfully developed a general method for synthesis of various Mn-based transition metal oxide twin-microspheres, including  $\text{Mn}_3\text{O}_4$ ,  $\text{CoMn}_2\text{O}_4$ ,  $\text{ZnMn}_2\text{O}_4$ ,  $\text{Ni}_x\text{Mn}_{3-x}\text{O}_4$ , and  $\text{Cu}_x\text{Mn}_{3-x}\text{O}_4$ ,  $\text{Fe}_x\text{Mn}_{3-x}\text{O}_4$ . The preparation strategy first involved synthesizing the twin-microspheres of metal carbonate precursor. Then, by the aid of thermal post-treatment in laboratory air at  $500\text{ }^\circ\text{C}$  for 4 h, the corresponding carbonate can topotactically convert to respective oxide twin-microspheres without changing the overall morphologies. As an example,  $\text{CoMn}_2\text{O}_4$  porous twin-microspheres are studied as an anode material for LIBs. Due to the unique mesoporous hierarchical

micro/nanostructures and the possible synergetic effects of different metal ions, the as-obtained  $\text{CoMn}_2\text{O}_4$  twin-microspheres exhibits excellent properties according to cycling performance and rate capability as well as cycle life for LIBs. Moreover, it should be noted that the method could be extended to synthesize of other metal oxides with novel hierarchical architecture.

### Acknowledgements

The authors gratefully acknowledge the financial supports provided by the National Basic Research Program of China (the 973 Project of China, No. 2011CB935901), National Natural Science Fund of China (No. 21371108), Shandong Provincial Natural Science Foundation for Distinguished Young Scholar (No. JQ201304), and the National Science Foundation of Shandong Province (No. ZR2012BM018).

### References

- 1 F. Y. Cheng, J. A. Shen, B. Peng, Y. D. Pan, Z. L. Tao, J. Chen, *Nat. Chem.* **2011**, *3*, 79.
- 2 G. Q. Zhang, X. W. Lou, *Angew. Chem. Int. Ed.* 2014, *53*, 9041; *Angew. Chem.* **2014**, *126*, 9187.
- 3 Y. M. Chiang, *Science* **2010**, *330*, 1485.
- 4 T. Brezesinski, J. Wang, S. H. Tolbert, B. Dunn, *Nat. Mater.* 2010, *9*, 146.
- 5 P. Simon, Y. Gogotsi, *Nat. Mater.* **2008**, *7*, 845.
- 6 J. R. Miller, P. Simon, *Science* **2008**, *321*, 651.
- 7 C. G. Morales-Guio, S. D. Tilley, H. Vrubel, M. Gratzel, X. L. Hu, *Nat. Commun.* **2014**, *5*, 3059.

- 8 G. Q. Zhang, L. Yu, H. B. Wu, H. E. Hoster, X. W. Lou, *Adv. Mater.* **2012**, *24*, 4609.
- 9 L. Hu, H. Zhong, X. R. Zheng, Y. M. Huang, P. Zhang, Q. W. Chen, *Sci. Rep.* **2012**, *2*, 986.
- 10 J. F. Li, S. L. Xiong, X. W. Li, Y. T. Qian, *Nanoscale* **2013**, *5*, 2045.
- 11 C. Z. Yuan, H. B. Wu, Y. Xie, X. W. Lou, *Angew. Chem. Int. Ed.* **2014**, *53*, 1488; *Angew. Chem.* **2014**, *126*, 1512.
- 12 X. W. Li, D. Li, L. Qiao, X. H. Wang, X. L. Sun, P. Wang, D. Y. He, *J. Mater. Chem.* **2012**, *22*, 9189.
- 13 B. Sun, Z. X. Chen, H. S. Kim, H. Ahn, G. X. Wang, *J. Power Sources* **2011**, *196*, 3346.
- 14 X. Q. Yu, Y. He, J. P. Sun, K. Tang, H. Li, L. Q. Chen, X. J. Huang, *Electrochem. Commun.* **2009**, *11*, 791.
- 15 X. W. Li, S. L. Xiong, J. F. Li, X. Liang, J. Z. Wang, J. Bai, Y. T. Qian, *Chem. Eur. J.* **2013**, *19*, 11310.
- 16 H. L. Wang, L. F. Cui, Y. Yang, H. S. Casalongue, J. T. Robinson, Y. Y. Liang, Y. Cui, H. J. Dai, *J. Am. Chem. Soc.* **2010**, *132*, 13978.
- 17 J. Gao, M. A. Lowe, H. D. Abruna, *Chem. Mater.* **2011**, *23*, 3223.
- 18 Z. C. Bai, N. Fan, Z. C. Ju, C. L. Guo, Y. T. Qian, B. Tang, S. L. Xiong, *J. Mater. Chem. A* **2013**, *1*, 10985.
- 19 G. Jian, Y. Xu, L. Lai, C. Wang, M. Zachariah, *J. Mater. Chem. A* **2014**, *2*, 4627.
- 20 Y. R. Liu, J. Bai, X. J. Ma, J. F. Li, S. L. Xiong, *J. Mater. Chem. A* **2014**, *2*, 14236.
- 21 Y. Y. Yang, Y. Q. Zhao, L. F. Xiao, L. L. Zhang, *Electrochem. Commun.* **2008**, *10*, 1117.
- 22 L. Zhou, H. B. Wu, T. Zhu, X. W. Lou, *J. Mater. Chem.* **2012**, *22*, 827.

- 23 C. Z. Yuan, J. Y. Li, L. R. Hou, L. H. Zhang, X. G. Zhang, *Part. Part. Syst. Charact.* **2014**, *31*, 657.
- 24 P. Poizot, S. Laruelle, S. Grugeon, L. Dupont, J. M. Tarascon, *Nature* **2000**, *407*, 496.
- 25 J. Bai, X. G. Li, G. Z. Liu, Y. T. Qian, S. L. Xiong, *Adv. Funct. Mater.* **2014**, *24*, 3012.
- 26 M. H. Oh, T. Yu, S. H. Yu, B. Lim, K. T. Ko, M. G. Willinger, D. H. Seo, B. H. Kim, M. G. Cho, J. H. Park, K. Kang, Y. E. Sung, N. Pinna, T. Hyeon, *Science* **2013**, *340*, 964.
- 27 X. Y. Lai, J. E. Halpert, D. Wang, *Energy Environ. Sci.* **2012**, *5*, 5604 .
- 28 X. W. Lou, L. A. Archer, Z. C. Yang, *Adv. Mater.* **2008**, *20*, 3987.
- 29 J. H. Sun, J. S. Zhang, M. W. Zhang, M. Antonietti, X. Z. Fu, X. C. Wang, *Nat. Commun.* **2012**, *3*, 1339.
- 30 J. B. Joo, Q. Zhang, M. Dahl, I. Lee, J. Goebel, F. Zaera, Y. D. Yin, *Energy Environ. Sci.* **2012**, *5*, 6321.
- 31 F. Li, F. L. Gong, Y. H. Xiao, A. Q. Zhang, J. H. Zhao, S. M. Fang, D. Z. Jia, *ACS Nano* **2013**, *7*, 10482.
- 32 Y. H. Xiao, S. J. Liu, F. Li, A. Q. Zhang, J. H. Zhao, S. M. Fang, D. Z. Jia, *Adv. Funct. Mater.* **2012**, *22*, 4052.
- 33 S. A. Needham, G. X. Wang, K. Konstantinov, Y. Tournayre, Z. Lao, H. K. Liu, *Electrochem. Solid-State Lett.*, **2006**, *9*, A315.
- 34 B. J. Tan, K. J. Klabunde, P. M. A. Sherwood, *J. Am. Chem. Soc.*, **1991**, *113*, 855.
- 35 J. F. Marco, J. R. Gancedo, M. Gracia, J. L. Gautier, E. I. Ríos, F.J. Berry, *J. Solid State Chem.* **2000**, *153*, 74.
- 36 T. Choudhury, S. O. Saied, J. L. Sullivan, A. M. Abbot, *J. Phys. D: Appl. Phys.* **1989**, *22*,

1185.

37 Y. E. Roginskaya, O. V. Morozova, E. N. Lubnin, Y. E. Ulitina, G. V. Lopukhova, S.

Trasatti, *Langmuir* **1997**, 13, 4621.

38 J. H. Zhong, A. L. Wang, G. R. Li, J. W. Wang, Y. N. Ou, Y. X. Tong, *J. Mater. Chem.*

**2012**, 22, 5656.

39 L. Zhou, D. Y. Zhao, X. W. Lou, *Adv. Mater.* **2012**, 24, 745.

40 G. Q. Zhang, X. W. Lou, *Angew. Chem. Int. Ed.* **2014**, 53, 9041.

41 F. M. Courtel, H. Duncan, Y. Abu-Lebdeh, I. J. Davidson, *J. Mater. Chem.* **2011**,

21,10206.

## Figures and Captions

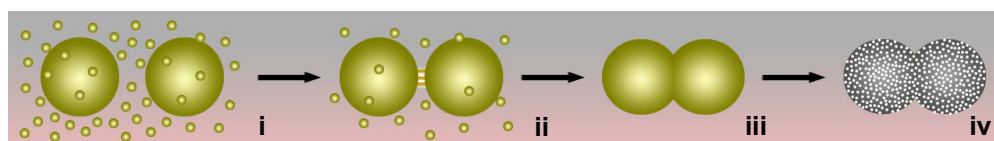


**Figure 1.** Schematic diagram illustrating the formation process of porous  $\text{CoMn}_2\text{O}_4$  twin microspheres.

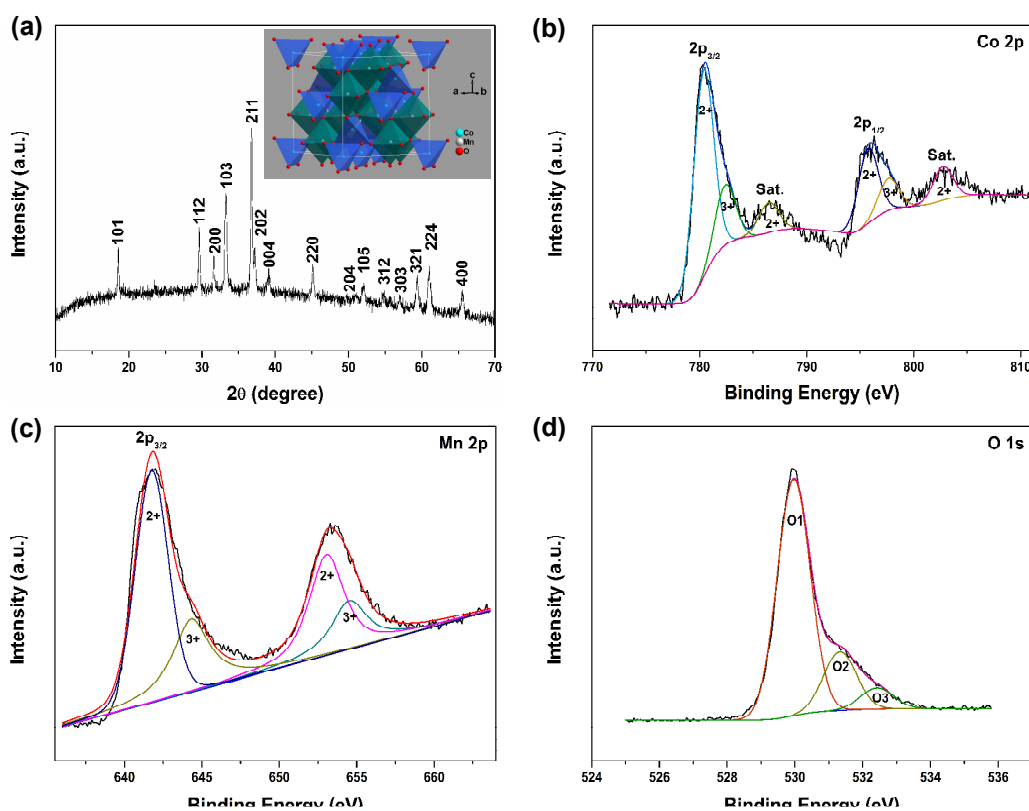


**Figure 2.** (a) XRD patterns of the as-prepared CoMn<sub>2</sub>O<sub>4</sub> twin microspheres; inset: the crystal structure of tetragonal spinel CoMn<sub>2</sub>O<sub>4</sub>. High-resolution XPS spectra of (b) Co 2p, (c) Mn 2p, and (d) O 1s for the CoMn<sub>2</sub>O<sub>4</sub> twin microspheres.

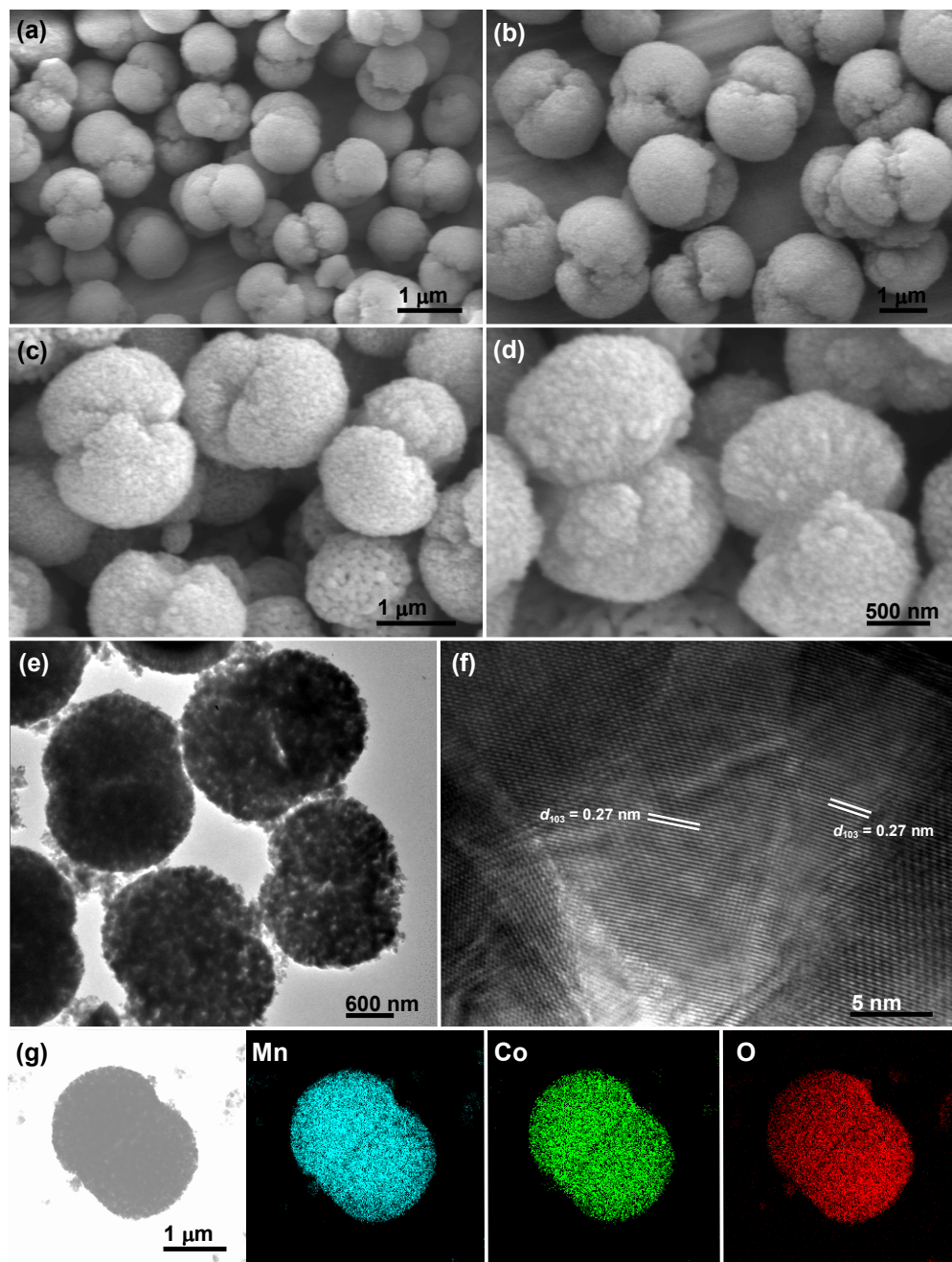


**Figure 3.** FESEM images of  $\text{Co}_{0.33}\text{Mn}_{0.67}\text{CO}_3$  twin microspheres (a,b); FESEM (c,d), TEM (e) and high-resolution TEM image (f) of  $\text{CoMn}_2\text{O}_4$  twin microspheres. (g) STEM image and the corresponding EDX elemental mappings of Mn, Co, and O for a single representative  $\text{CoMn}_2\text{O}_4$  twin microsphere.

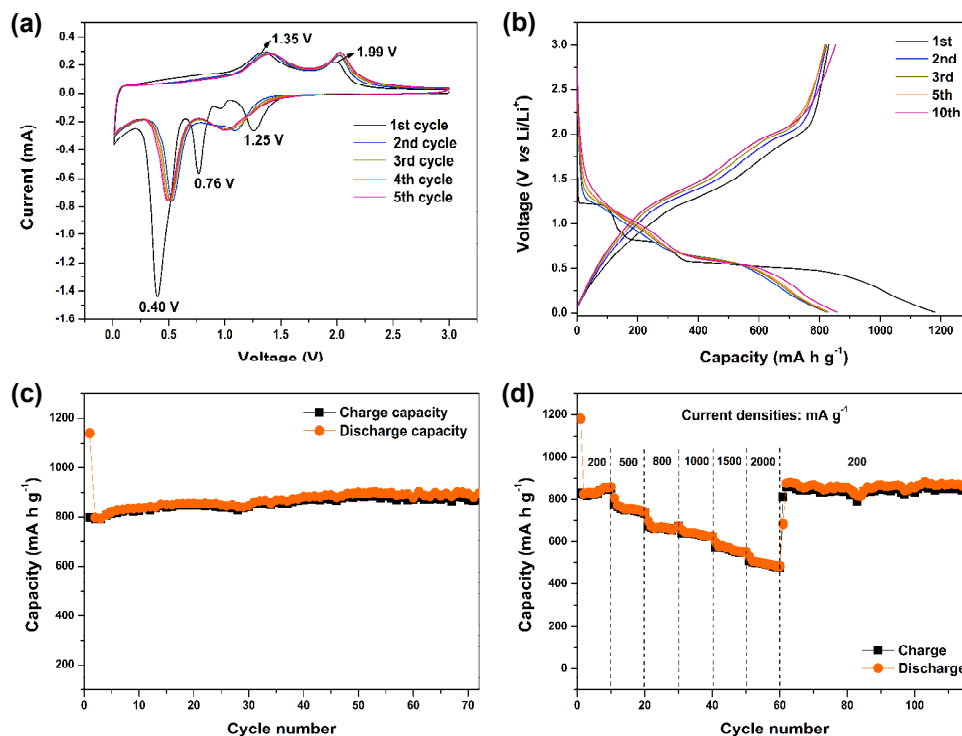


**Figure 4.** Electrochemical evaluation of  $\text{CoMn}_2\text{O}_4$  twin microspheres for anode of lithium-ion batteries: a) Cyclic voltammetry (CV) curves at a scan rate of  $0.1 \text{ mV s}^{-1}$  in the voltage window of  $0.01\text{--}3.0 \text{ V}$ ; b) discharge-charge voltage profiles and c) cycling performance recorded at a current density of  $200 \text{ mA g}^{-1}$ ; d) rate capability at different current densities between  $0.01$  and  $3.0 \text{ V}$ .

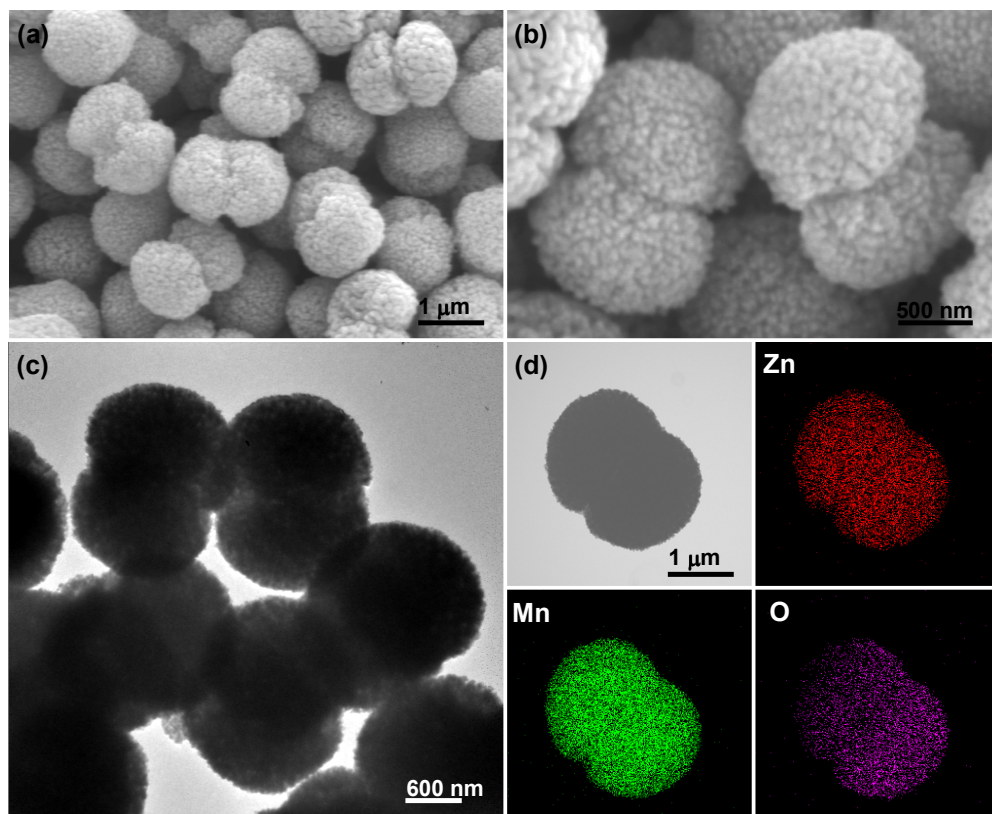


**Figure 5** (a,b) FESEM images of  $\text{Mn}_3\text{O}_4$  twin microspheres. (c,d) TEM images of  $\text{ZnMn}_2\text{O}_4$  twin microspheres, STEM image and the corresponding EDX elemental mappings of Zn, Mn, and O for a single representative  $\text{ZnMn}_2\text{O}_4$  twin microsphere.

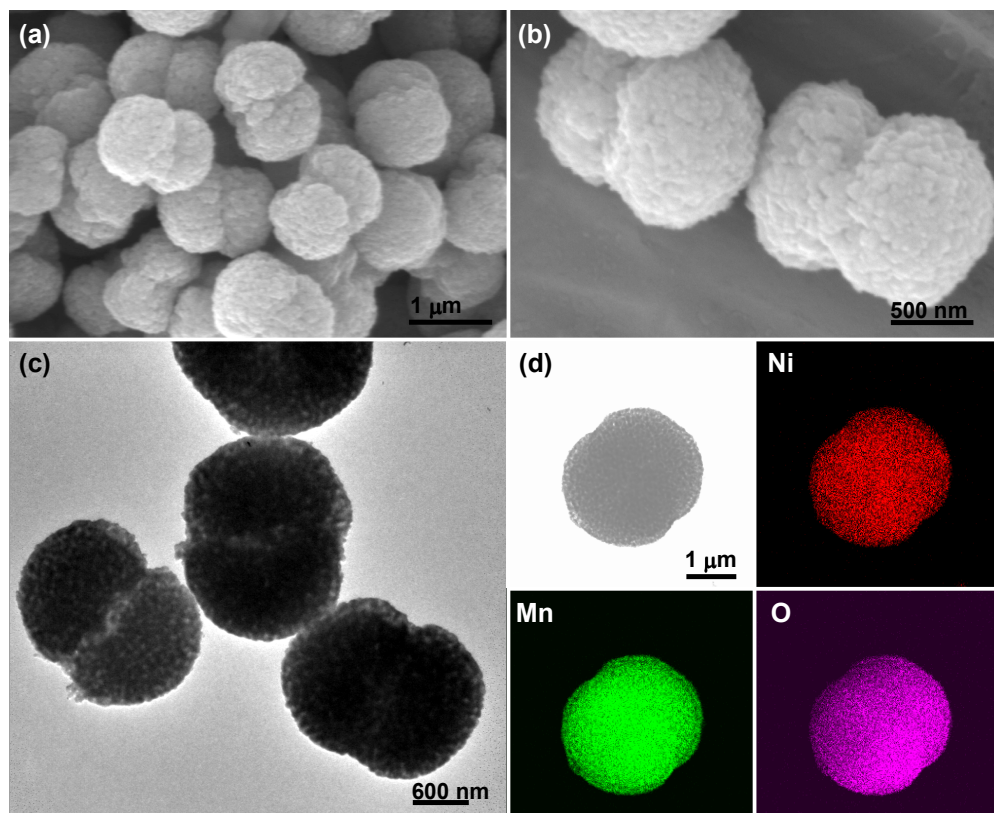


**Figure 6.** FESEM (a,b) and TEM (c) of  $\text{Ni}_x\text{Mn}_{3-x}\text{O}_4$  twin microspheres. (d) STEM image and the corresponding EDX elemental mappings of Ni, Mn, and O for a single representative  $\text{Ni}_x\text{Mn}_{3-x}\text{O}_4$  twin microsphere.

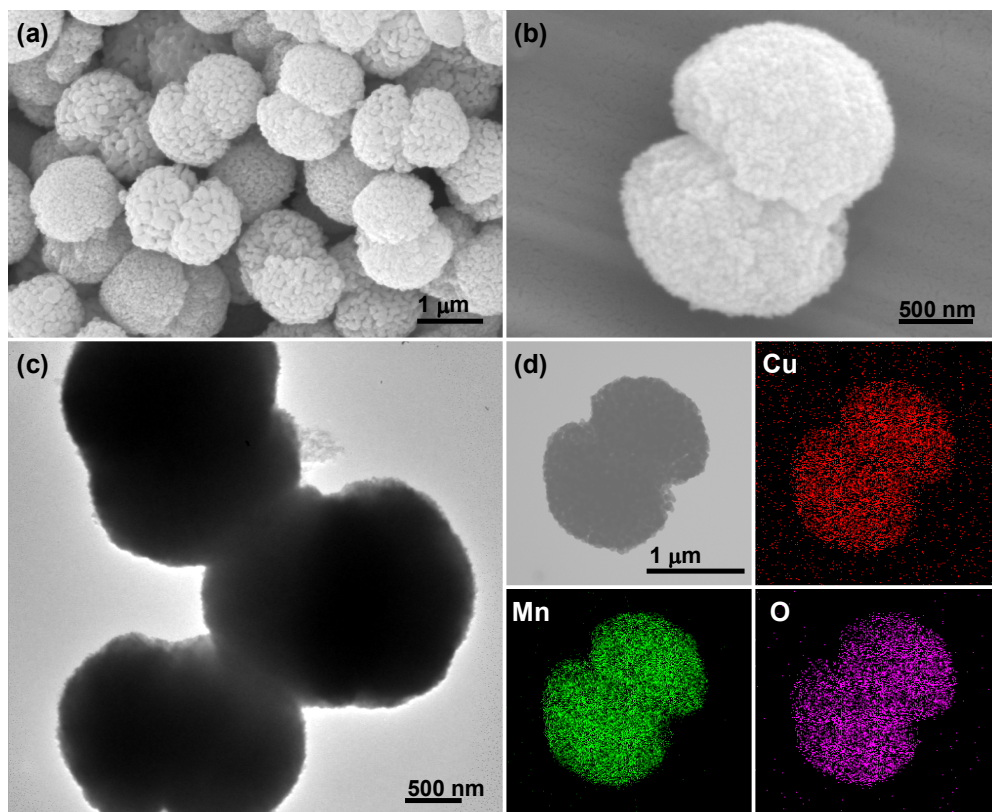


**Figure 7.** FESEM (a,b) and TEM (c) of  $\text{Cu}_x\text{Mn}_{3-x}\text{O}_4$  twin microspheres. (d) STEM image and the corresponding EDX elemental mappings of Cu, Mn, and O for a single representative  $\text{Cu}_x\text{Mn}_{3-x}\text{O}_4$  twin microsphere.

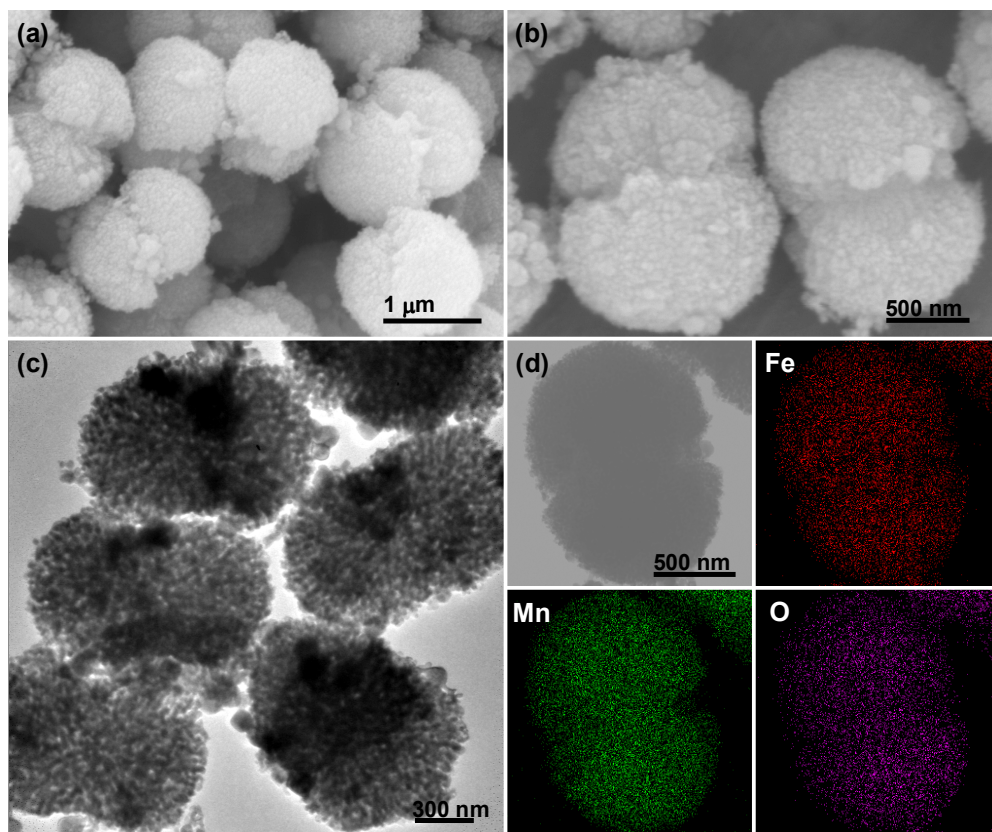


**Figure 8.** FESEM (a,b) and TEM (c) of  $\text{Fe}_x\text{Mn}_{3-x}\text{O}_4$  twin microspheres. (d) STEM image and the corresponding EDX elemental mappings of Fe, Mn, and O for a single representative  $\text{Fe}_x\text{Mn}_{3-x}\text{O}_4$  twin microsphere.